Larhyss Journal, ISSN 1112-3680, n°66, Jun 2026, pp. 7-30

EFFECTS OF SURFACE GRAVITY WAVES ON RIGID DAMS

***TADJADIT A.*[1]*, *DELLIL H.*[2]**

[1] Associate Professor, Laboratory of seismic engineering and structural dynamics (LGSDS), National polytechnic school, Hacen Badi Avenue, El harrach 16200, Algiers, Algeria
[2] Civil Engineer, Department of Civil Engineering, National polytechnic school, Hacen Badi Avenue, El harrach 16200, Algiers, Algeria

(*) abdelmadjid.tadjadit@g.enp.edu.dz

Research Article – Available at http://larhyss.net/ojs/index.php/larhyss/index
Received June 15, 2025, Received in revised form May 26, 2026, Accepted May 28, 2026

ABSTRACT

This study, based on two-dimensional flow theory, focuses on calculating and analyzing the effects of surface gravity waves on the hydrodynamic pressure distribution of a partially inclined rigid dam subjected to short-term horizontal harmonic excitation at its base, considering the combined effects of surface gravity waves, fluid compressibility, and viscosity within a unified Trefftz-based semi-analytical framework, with a detailed parametric investigation of their coupled influence on hydrodynamic forces. The Trefftz numerical method is used to solve the reduced wave equation. The advantage of this boundary value calculation approach lies in limiting the number of unknowns to the number of Trefftz test functions. Thus, the computational effort is independent of the reservoir area.

The unknown coefficients of the problem are obtained by a continuous least-squares treatment of the unsatisfied boundary condition at the dam-reservoir interface. The Newton-Raphson method is then applied to numerically solve the transcendental dispersion relation, thereby integrating the effects of surface gravity waves. The results obtained concern hydrodynamic pressures, shear forces, and the corresponding overturning moments.

The effects of surface waves are particularly evident at low frequencies. Although significant, they remain less influential than the inclination of the upstream face. The combined effect is also evaluated. At low frequencies, a substantial reduction in pressure forces is observed. However, as the excitation frequency increases, the effect of surface waves gradually diminishes, giving way to the effects of viscous damping, which becomes apparent near resonant frequencies and significantly reduces the resonance peaks. The results from this approach are very consistent with the trends reported in the specialized literature.

Keywords: Two-dimensional flow theory, Harmonic excitation, Rigid dam, Surface gravity waves, Hydrodynamic pressures, Trefftz numerical method.

INTRODUCTION

Earthquake-induced hydrodynamic forces on the upstream face of dams are a critical consideration in the safe design of hydraulic structures in seismic regions. The classical solution for hydrodynamic pressure on a rigid dam with a vertical upstream face under horizontal ground motion was first derived by (Westergaard, 1933). Since then, numerous researchers have extended this model to incorporate additional physical effects, such as fluid compressibility (Chopra, 1967), reservoir bottom absorption (Hall and Chopra, 1972; Fenves and Chopra, 1984; Zegait and Pizzo, 2023; Verma et al., 2023; Shaikh et al., 2024; Belouz et al., 2025), dam flexibility (Tiliouine and Seghir, 1998), and surface gravity waves (Chwang, 1981; Wu and Yu, 1989; Avilés and Suárez, 2010).

The geometry of the dam-reservoir interface has also been shown to strongly influence the hydrodynamic pressure distribution (Remini and Toumi, 2017; Mezenner et al., 2022; Mehta et al., 2023; Panchal and Suryanarayana, 2025). Chwang (1978) provided an exact solution for dams with inclined upstream faces under constant reservoir depth, although surface waves were neglected. Liu (1986) generalized this approach to triangular reservoirs. However, these exact solutions, often based on Schwarz-Christoffel conformal mapping, are limited to simple geometries and cannot capture free-surface dynamics.

Later, Avilés and Sanchez-Sesma (1986) employed a Trefftz-based boundary method to study inclined faces, showing its accuracy and simplicity. Their results supported Zangar's experimental observations that inclined faces reduce hydrodynamic pressures compared to vertical faces.

Research on surface gravity waves has highlighted their significant role in modifying dam-reservoir interaction (Ghouini et al., 2024). Chwang (1981) emphasized the importance of free-surface oscillations in hydrodynamic analyses. Wu and Yu (1989) applied the Trefftz method to evaluate surface-wave effects on dams with arbitrary upstream faces, assuming an incompressible and inviscid fluid. Their work demonstrated that wave motion can significantly modify the pressure field and force distribution along the dam face. More recently, Avilés and Suárez (2010) investigated compressibility and viscosity effects for arbitrary upstream faces. However, the coupled parametric influence of surface waves, inclination, and viscous damping on pressures, forces, and overturning moments has not been systematically investigated. In parallel, Da Silva and Pedroso (2019) provided an exact solution to Laplace's equation for dams with flat vertical faces, explicitly distinguishing between conservative inertial effects and dissipative surface-wave contributions, both governed by the Froude number.

Although the Trefftz method and the inclusion of compressibility and viscosity were previously introduced by Avilés and Sánchez-Sesma (1986) and Avilés and Suárez (2010), the present study extends these works by providing a detailed parametric investigation of the coupled effects of surface gravity waves, fluid viscosity, and upstream

face inclination on hydrodynamic pressures, shear forces, and overturning moments. Furthermore, the dispersion relation is solved numerically using the Newton–Raphson technique, enabling an accurate assessment of wave-induced resonant effects.

The objective of the present study is to address this gap by developing a semi-analytical formulation based on the Trefftz method that jointly incorporates surface gravity waves, fluid compressibility, and viscosity for rigid dams with partially inclined upstream faces subjected to horizontal harmonic excitation. The approach employs analytical expressions previously validated by Tadjadit and Tiliouine (2018) and introduces the surface-wave dispersion relation, solved numerically using the Newton-Raphson method. This enables efficient computation of hydrodynamic pressures, shear forces, and overturning moments, and provides new insights into the relative contributions of surface waves, inclination, and viscous damping across different frequency regimes.

FORMULATION OF THE PROBLEM

Assumptions

A rigid, partially inclined dam undergoes horizontal ground acceleration, denoted as $\ddot{x}_g$, shown in Fig. 1. The dam's response is modeled in a two-dimensional system with an infinitely long reservoir with a horizontal rigid bottom.

The water is considered linearly compressible and viscous. The flow is modeled using a potential-flow formulation with an equivalent linear viscous damping representation, which is commonly adopted in dam-reservoir interaction analyses. In this study, harmonic base excitation is adopted to derive a closed-form frequency-domain solution and to investigate resonance mechanisms. This simplified excitation is commonly used in fundamental dam–reservoir interaction research. Extension to real earthquake records can be achieved through Fourier decomposition. In the present formulation, viscosity is introduced through a linear viscoelastic (Kelvin-Voigt) representation leading to a complex-valued effective wave parameter, which accounts for internal damping while preserving the linear potential flow framework under small perturbations. Similar modeling strategies have been adopted in dam–reservoir interaction analyses (Avilés and Li, 1998; Avilés and Suárez, 2010).

Let H_r, denote the total reservoir depth. The inclined portion begins at a height $H_f = c\, H_r$, where $c \in [0, 1]$ and forms an angle θ with the vertical. This setup follows the assumptions of Tadjadit and Tiliouine (2018), in which a semi-analytical approach via the Trefftz method is employed. The flow is expressed through a velocity potential function Φ, which satisfies the governing wave equation. This formulation simplifies the treatment of boundary conditions and is well suited to the Trefftz framework. The free surface condition is treated with or without considering the effect of surface gravity waves.

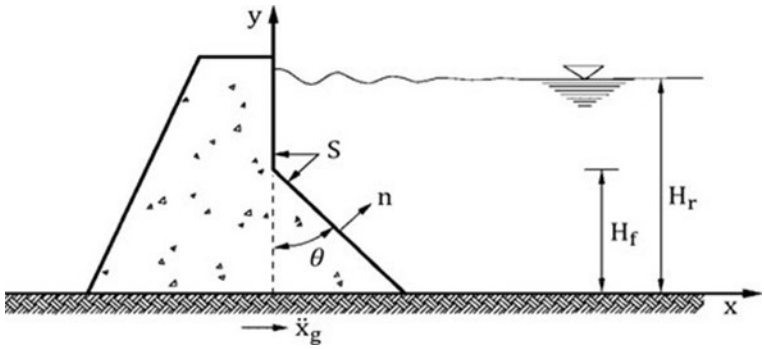

Figure 1: Rigid partially inclined dam subject to horizontal harmonic excitation

The harmonic movement of water is assumed small and irrotational, allowing the flow field in the two-dimensional reservoir to be expressed by a velocity potential function Φ that satisfies the reduced wave equation:

$$\frac{\partial^2 \Phi}{\partial x^2} + \frac{\partial^2 \Phi}{\partial y^2} + k\,\Phi = 0 \tag{1}$$

Where the complex wave parameter k accounts for compressibility and viscoelastic damping effects without introducing rotational flow components. The velocity potential Φ is related to the velocities of the fluid particles and the hydrodynamic pressure through:

$$\dot{u} = -\frac{\partial \Phi}{\partial x}, \dot{v} = -\frac{\partial \Phi}{\partial y}, p = \rho \frac{\partial \Phi}{\partial t} \tag{2}$$

$\dot{u}$ and $\dot{v}$ are the particle velocities in the x and y directions, respectively, p is the hydrodynamic pressure in the liquid and $k = \omega/C$ is the wavelength parameter of the internal compression waves. Here, ω is the angular frequency of excitation and $C = \sqrt{(\lambda / \rho)}$ the velocity of compression waves in water, with λ being Lamé's modulus and ρ mass density of water. In the incompressible limit ($C \to \infty$ *that implies* $k \to 0$), Eq. (1) reduces to Laplace equation:

$$\nabla^2 \Phi = 0 \tag{3}$$

Which is the form adopted in classical incompressible analyses (e.g., Wu and Yu, 1989).

Boundary conditions

For an infinitely long dam-reservoir system subjected to horizontal ground motion, the boundary conditions in the frequency domain are as follows:
the crest, less so near full height.

Free surface condition

On the free surface, Poisson's boundary condition for surface gravity waves is applied:

$$\left(\frac{\partial^2 \Phi}{\partial t^2} + g \frac{\partial \Phi}{\partial y} \right) \Big|_{y = H_r} = 0 \tag{4}$$

Where g is the acceleration due to gravity. For scenarios without surface wave effects, a pressure-free condition is assumed on the free surface of the reservoir (Avilés and Li, 1998; Tadjadit and Tiliouine, 2018). This condition is explicitly given as follows, while velocity potential is fixed at a constant value:

$$\left(\frac{\partial \Phi}{\partial t} \right) \Big|_{y = H_r} = 0 \tag{5}$$

Rigid bottom condition

For a reservoir with rigid bottom, the vertical particle velocity is:

$$\left(\frac{\partial \Phi}{\partial y} \right) \Big|_{y = 0} = 0 \tag{6}$$

Radiation condition

The radiation condition at infinity is:

$$\lim_{x \to \infty} \Phi = 0 \tag{7}$$

Dam upstream face condition

For a rigid dam with a non-vertical upstream face, the normal velocity of the particles of water in contact with the dam is equal to that of the upstream dam face (Normal gradient of the velocity potential fixed at a constant value):

$$\left(\frac{\partial \Phi}{\partial n} \right) \Big|_S = -\dot{x}_n \tag{8}$$

Here, n is the outward normal direction to the upstream face, S is the dam-water interface, and:

$$\dot{x}_n = \begin{cases} \dot{x}_g \cos\theta \ , & y \le H_f \\ \dot{x}_g \ , & y \ge H_f \end{cases} \tag{9}$$

Viscous fluid model

Assuming small deformations and accounting for both compressibility and viscosity of the reservoir fluid, we adopt the linear viscoelastic Kelvin-Voigt model (Avilés and Li, 1998; Tadjadit and Tiliouine, 2018) to represent internal loss energy. In this formulation, Lamé's modulus is replaced by a frequency-dependent complex expression that captures viscous damping in wave propagation. It is defined as:

$$\lambda^c = \lambda\left(1 + i\,2\,\xi\,\eta\right) \tag{10}$$

Where ξ is the viscous damping ratio and $\eta = \omega H_r/C$ the dimensionless frequency. This compact representation efficiently models energy loss due to internal dissipation and attenuation of compression waves propagating away from the dam. (Avilés and Li, 1998; Tadjadit, 2024).

Solution by Trefftz method

To solve the governing equation, a semi-analytical approach based on the Trefftz method is adopted. Since the governing equation is formulated in terms of the velocity potential Φ, the general solution is expressed in the frequency domain as a linear combination of Trefftz functions *T (x, y, ω).* Accordingly, it can be expanded as:

$$\Phi\left(x, y, \omega\right) = \dot{x}_g \sum_{j=1}^{\infty} \phi_j \, T_j\left(x, y, \omega\right) \tag{11}$$

Where, φ_j are complex-valued coefficients to be determined for the remaining boundary condition at the upstream face. Following the semi-analytical framework developed by Tadjadit and Tiliouine (2018), only the final algebraic system is presented here for completeness:

$$\left[F_{ij}\right]\left\{\phi_j\right\} = \left\{G_i\right\}, \qquad i, j = 1, 2, \ldots, \infty \tag{12}$$

Where, the matrix components are defined by:

$$F_{ij} = \int_S \frac{\partial T_i^*}{\partial n} \frac{\partial T_j}{\partial n} \, ds \tag{13}$$

$$G_i = -\int_S \frac{\dot{x}_n}{\dot{x}_g} \frac{\partial T_j^*}{\partial n} ds \tag{14}$$

The elements of the Hermitian matrix $[F_{i\,j}]$ and the column vector $\{G_i\}$ are calculated analytically as defined in Eq. (13) and Eq. (14), yielding closed-form expressions. Because the Trefftz expansion involves an infinite number of terms, the system Eq. (12) must be truncated to a finite number of basic functions. To do this, we considered a tolerance of 10^{-4}. The Trefftz derivable and continuous functions are constructed to satisfy the governing equation as well as the boundary conditions at the free surface, reservoir bottom, and at infinity. Using separation of variables, the natural modes of horizontal internal wave propagation are expressed as:

$$T_j\left(x, y, \omega\right) = e^{-\mu_j x} \cos\left(\lambda_j y\right) \tag{15}$$

μ_j and λ_j are, respectively, horizontal and vertical propagation constants. For a dissipative fluid, μ_j is a complex-valued quantity in general (Avilés and Suarez, 2010).

Derivation of vertical propagation constants λ_j. The vertical propagation constants λ_j for the Trefftz functions are determined from the free-surface conditions introduced in Eqs. (4) and Eq. (5). Two cases arise:

$$\mu_j = \sqrt{\lambda_j^{\,2} - k^2} \tag{16}$$

Case 1: with surface gravity waves

Using the dynamic free-surface condition Eq. (4), the dispersion relation governing becomes:

$$\lambda_j H_r \tan\left(\lambda_j H_r\right) = -\sigma \tag{17}$$

Where σ is the surface-wave parameter defined later in Eq. (31). A demonstration of this equation is provided in Appendix A. A similar dispersion relation was previously used by Wu and Yu (1989), who analyzed the same free surface condition in an incompressible, inviscid fluid. Their formulation introduced the parameter $CW = g/\omega^2 H_r$, which is simply the reciprocal of our notation σ. Eq. (17), is solved iteratively using the Newton-Raphson method (see below the section relating to this method). For $\sigma = 0$, the roots are $\lambda_j H_r = j\,\pi$, while for $\sigma \to \infty$, the roots are $\lambda_j H_r = (2j - 1)\,\pi/2$.

Case 2: without surface gravity waves

Applying the pressure-release condition at the free surface Eq. (5) leads directly to:

$$\lambda_j = \frac{(2j-1)\,\pi}{2\,H_r} \tag{18}$$

Thus, the form of λ_j depends only on whether surface-wave effects are included Eq. (17) or neglected Eq. (18).

The Newton–Raphson method

The dispersion relation Eq. (17) is solved iteratively using the Newton-Raphson method (Deuflhard, 2011). This classical root-finding technique employs an initial estimate (X_n) and the tangent line of the function $f(X)$ to find a better approximation (X_{n+1}) using the formula:

$$X_{n+1} = X_n - \frac{f(X_n)}{f'(X_n)} \tag{19}$$

Where the function and its derivative are defined as:

$$f(X) = X\tan X + \sigma, \qquad f'(X) = \tan X + X\sec^2 X \tag{20}$$

With, $X = \lambda_j H_r$ iteration continues until convergence is reached, i.e., the difference between successive approximations falls below the tolerance of 10^{-7} used in this study.

Analytical expressions

Hydrodynamic pressures p (x, y, ω)

From Eq. (2), Eq. (11), and Eq. (15), the hydrodynamic pressure is given as:

$$p(x,y,\omega) = \rho\,\ddot{x}_g \sum_{j=1}^{\infty} \phi_j\, e^{-\mu_j x} \cos\lambda_j\, y \tag{21}$$

According to Eq. (21), at the dam-reservoir interface ($x = 0$), the hydrodynamic pressure distribution is defined as a function of height y. For a computational tolerance of 10^{-4}, beyond 25 terms, the uniform convergence of the series of the function p (y) is verified through the "Uniform Cauchy criterion". The latter converges to a function called "Limit function". Thus, under the above conditions, an approximate solution will be obtained for Eq. (21) for a finite number of terms (Tadjadit and Tiliouine, 2018).

Shear forces $F_h(y)$

The resultant horizontal shear force per unit dam length $F_h(y)$, acting along the dam face at a given depth y, is obtained by integrating the hydrodynamic pressure over the dam-water interface (Tadjadit and Tiliouine, 2018):

$$F_h(y) = \int_S C_s \gamma H_r C_p(y) ds \tag{22}$$

where ds represents an infinitely small segment of the contour S, C_s is the normalized ground acceleration, C_p is the normalized pressure coefficient, and $\gamma = \rho g$ the unit weight of water. Closed-form analytical expressions for $F_h(y)$ can be obtained for the partially inclined dam face.

For $0 \le y \le c\,H_r$:

$$F_h(y) = \sum_{i=1}^{\infty} A_i \left[-e^{a_i(c H_r - y)} F_i(y) + F_i(c H_r) + \frac{\sin(\lambda_i H_r) - \sin(\lambda_i c H_r)}{\lambda_i} \right] \tag{23}$$

In addition, for $c\,H_r \le y \le H_r$:

$$F_h(y) = \sum_{i=1}^{+\infty} A_i \left\{ \frac{\sin(\lambda_i H_r) - \sin(\lambda_i y)}{\lambda_i} \right\} \tag{24}$$

With:

$$A_i = \rho \ddot{x}_g \phi_i , \qquad F_i(y) = \left(\lambda_i \sin \lambda_i y + \mu_i \tan\theta \cos \lambda_i y \right) / \alpha_i^{+} \tag{25}$$

$$a_i = \mu_i \tan\theta, \qquad \alpha_i^{+} = \lambda_i^2 + a_i^2 , \quad \alpha_i^{-} = \lambda_i^2 - a_i^2 \tag{26}$$

Overturning moments $M_z(y)$

The overturning moment about the z- axis at depth y is defined from the shear force distribution as indicated by Tadjadit and Tiliouine (2018):

$$M_z(y) = \int_S F_h(y)\, ds \tag{27}$$

Analytical expressions are again obtained for a partially inclined dam.

For $0 \le y \le c\,H_r$:

$$M_z(y)=\sum_{i=1}^{+\infty} A_i \left\{ e^{-a_i\left(cH_r - y\right)} M_i(y) - M_i\left(cH_r\right) + \left(cH_r - y\right)\left[\frac{\lambda_i \sin\left(\lambda_i cH_r\right) + a_i \cos\left(\lambda_i cH_r\right)}{\alpha_i^{+}} + \frac{\sin\left(\lambda_i H_r\right) + \sin\left(\lambda_i cH_r\right)}{\lambda_i} \right] + \frac{\lambda_i H_r (1-c) \sin\left(\lambda_i H_r\right) - \cos\left(\lambda_i cH_r\right)}{\lambda_i^{2}} \right\} \quad (28)$$

In addition, for:

$$cH_r \le y \le H_r$$

The following can be written:

$$M_z(y)=\sum_{i=1}^{+\infty} A_i \left[\frac{\lambda_i \left(H_r - y\right)\sin\left(\lambda_i H_r\right) - \cos\left(\lambda_i y\right)}{\lambda_i^{2}} \right] \quad (29)$$

With:

$$M_i(y)=\frac{m_i \sin\lambda_i y + n_i \cos\lambda_i y}{\alpha_i^{+2}},\ m_i = 2\lambda_i a_i\ ,\ n_i = -\alpha_i^{-} \quad (30)$$

According to Eq. (21), at the dam-reservoir interface ($x = 0$), the hydrodynamic pressure For convenience in presenting the results, the magnitudes of the shear-force and overturning-moment coefficients are defined as follows:

$$C_f=\frac{\left|F_h\right|}{\gamma H_r^{2}},\qquad C_M=\frac{\left|M_z\right|}{\gamma H_r^{3}} \quad (31)$$

These coefficients, C_f and C_M, will be used in the results section to present the variation of hydrodynamic response with excitation frequency, damping ratio, dam-face inclination, and surface gravity waves.

RESULTS AND INTERPRETATION

The following section presents the numerical results obtained by applying the semi-analytical method described above. The parameters adopted for the dam-reservoir system are as follows: The depth of the reservoir H_r = 100 m, the propagation speed of compression waves in water C = 1438 m/s and the density of water ρ = 1000 kg/m³.

Results

At first, the results from the analytical formulation are validated against the exact solution proposed by Wu and Yu (1989) for the case of an incompressible, inviscid fluid (Fig. 2). To do this, the excitation frequency is expressed as a function of the CW wave-effect parameter as defined by Chwang (1981):

$$CW = \frac{g}{\omega^2 H_r} \tag{32}$$

Then, for a more complex case, a comparison with those from the solution of Avilés and Suárez (2010) was carried out for the case of a compressible and viscous fluid subjected to horizontal ground acceleration (Fig. 5). The coefficients of the shear forces and the corresponding overturning moments for both cases are presented. Additionally, the trends reported by Da Silva and Pedroso (2019) are summarized in Table 3. While Table 1 presents the maximum hydrodynamic pressure coefficients C_p^{max} obtained for an incompressible inviscid fluid (Wu and Yu, 1989), with values of the wave-effect parameter between CW = 0 and CW = 0.4.

Table 1: Maximum pressure coefficient C_p^{max} for a vertical and fully inclined dam under different surface-wave parameters and slope angles, assuming an incompressible inviscid fluid

θ°	CW	σ	C_p^{max} Without wave	C_p^{max} With wave	Relative deviation (Wave effect)	Relative deviation (combined effect)
0	0	∞	-	-	-	-
	0.2	5	0.742623	0.560585	24.51	-
	0.3	3.33	0.742623	0.439258	40.85	-
	0.4	2.5	0.742622	0. 328128	55.81	-
15	0	∞	-	-	-	-
	0.2	5	0.610471	0.524688	14.05	29.35
	0.3	3.33	0.610471	0.461041	24.47	37.91
	0.4	2.5	0.610471	0. 378215	38.04	49.07

30	0	∞	-	-	-	-
	0.2	5	0.504970	0.429557	14.93	42.15
	0.3	3.33	0.504964	0.409899	18.82	44.8
	0.4	2.5	0.504977	0.384060	23.94	48.28

The convergence of the present solution toward the exact solution of Wu and Yu (1989), for $CW = 0.2$ and $CW = 0.3$, is shown in Fig. 2

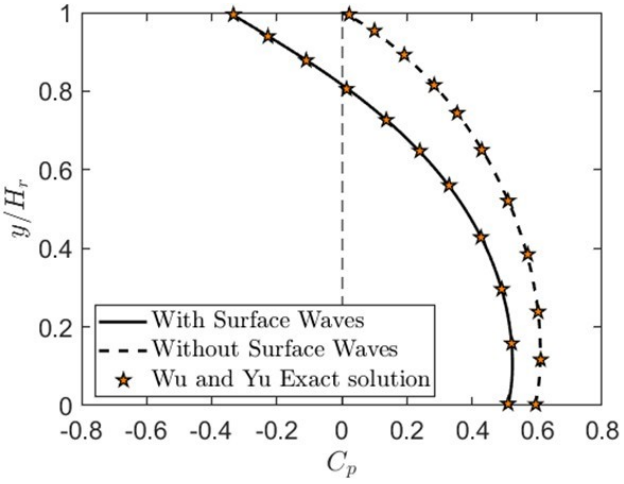

(a)

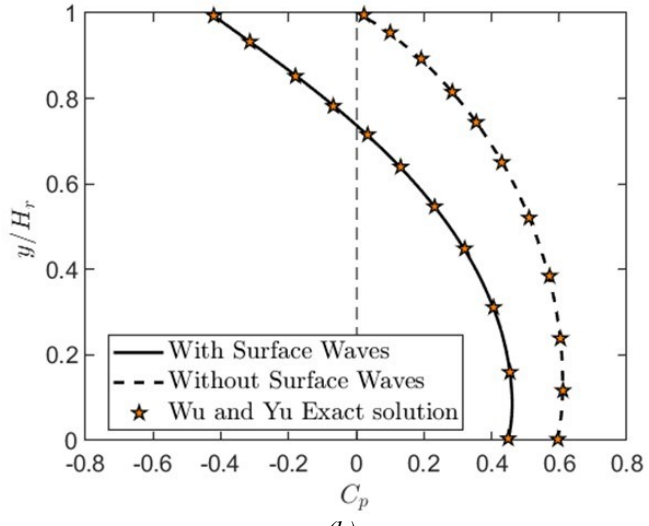

(b)

Figure 2: Convergence of the present solution toward the Wu and Yu (1989) exact solution for $c = 1$, $\theta = 15°$: (a) Case of $CW = 0.2$, (b) Case of $CW = 0.3$

Figs. 3 and 4 show the normalized pressure curves for the vertical and inclined dam cases ($\theta = 15°$), respectively.

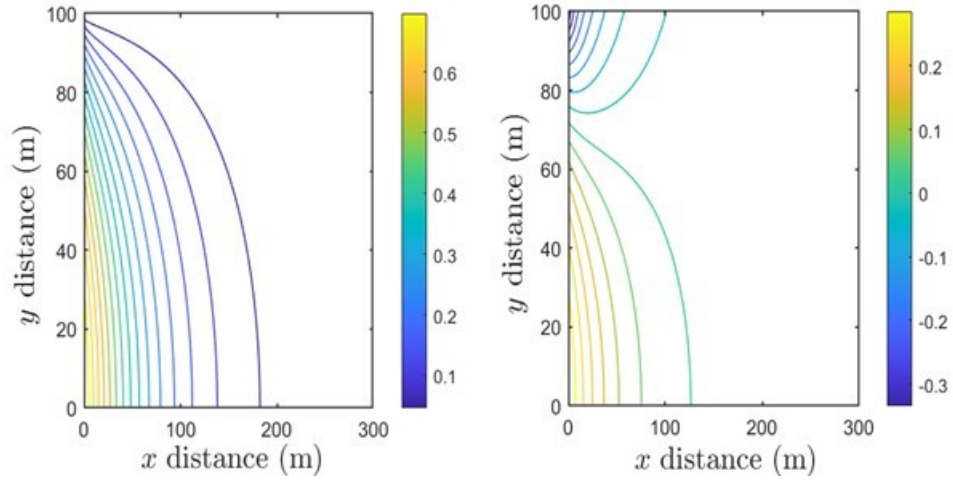

(a)

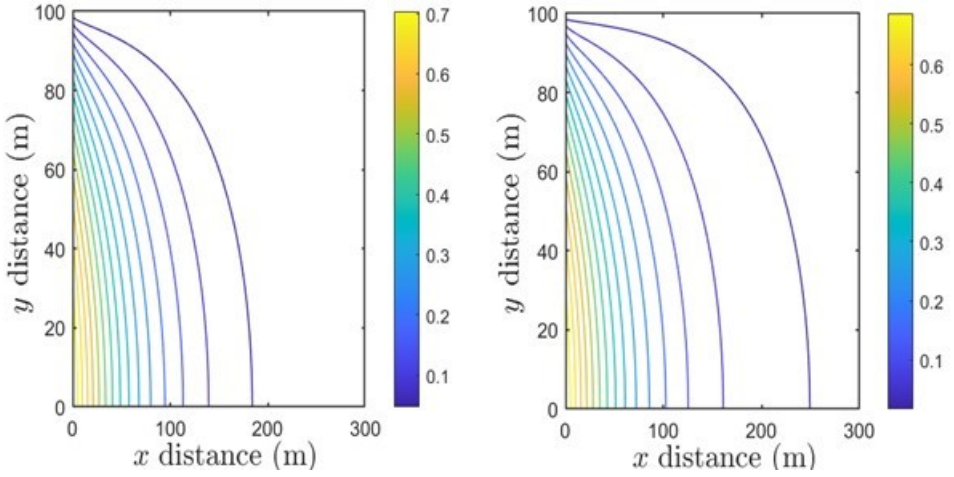

(b)

Figure 3: Shape of the normalized hydrodynamic pressure curves for $c = 0$, $\theta = 0°$, and $\xi = 1\%$: (a) Low excitation frequency, $\omega = 0.49$ rad/s; (b) High excitation frequency, $\omega = 3.13$ rad/s; left: without surface-wave effect, right: with surface-wave effect

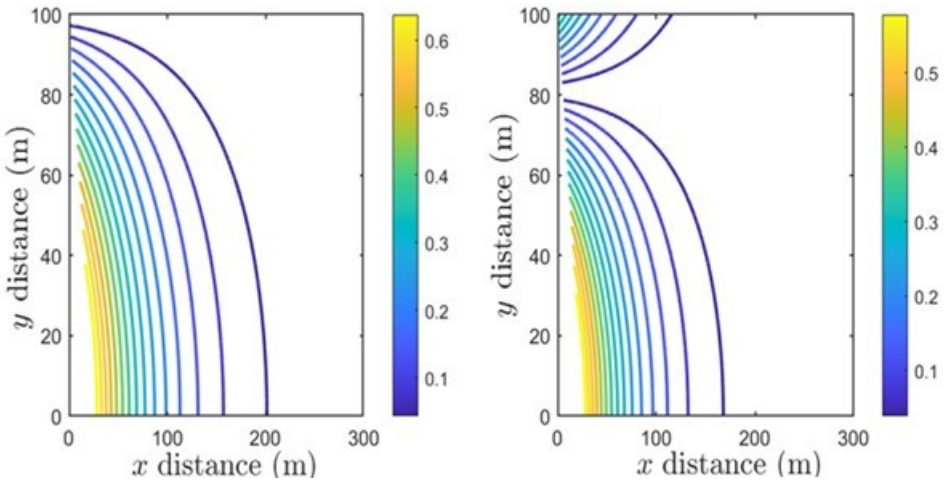

(a)

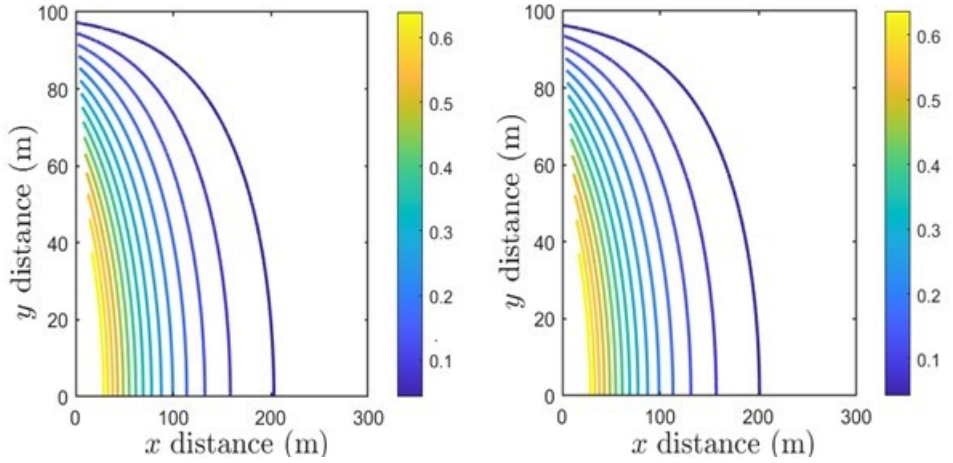

(b)

Figure 4: Shape of the normalized hydrodynamic pressure curves for $c = 1$, $\theta = 15°$, and $\xi = 1\%$: (a) Low excitation frequency, $\omega = 0.49$ rad/s, (b) High excitation frequency, $\omega = 3.13$ rad/s; left: without surface-wave effect, right: with surface-wave effect

Table 2: Comparison of C_p^{max} with and without surface waves effects for a compressible viscous fluid: $c = 1$, $\theta = 15°$, $\xi = 2\%$ and for different frequencies

$\theta°$	ω (rad/sec)	$C_p^{\max}$ (with wave)	$C_p^{\max}$ (Without wave)	Relative deviation %
15	0.49	0.378273	0.610524	+ 38.04
	0.70	0.524857	0.610664	+ 14.05
	1.71	0.596426	0.596532	- 0.0178
	2.20	0.597579	0.597685	- 0.0177
	3.13	0.616039	0.616103	- 0.0104

Table 2, presents the maximum hydrodynamic pressures C_p^{max} for a compressible viscous fluid at $\theta = 15°$ for different excitation frequencies ω.

According to Da Silva and Pedroso (2019), the total hydrodynamic response can be decomposed into two parts:

(1) A conservative component, associated with added mass and inertial effects,

(2) A dissipative component, linked to damping caused by surface gravity waves.

The relevance of these contributions depends on the Froude number F_r^2, which is equivalent to the surface-wave parameter σ:

$$F_r{}^2 = \sigma = \frac{1}{CW} = \frac{\omega^2 H_r}{g} \tag{33}$$

Slow regime $F_r{}^2 < 1$

Gravitational forces dominate, and the effect of surface gravity waves constitutes the main component of the hydrodynamic response.

Fast regime $F_r{}^2 > 1$

In contrast, as F_r^2 increases, inertial forces dominate, and the effect of surface gravity waves rapidly diminishes.

Table 3: Comparison of pressure coefficients with and without surface wave effects in slow and fast regimes

$F_r^2 < 1$ (Slow Regime)				$F_r^2 > 1$ (Fast Regime)			
σ	C_p^{max} (with wave)	C_p^{max} (without wave)	Percentage deviation (%)	σ	C_p^{max} (with wave)	C_p^{max} (without wave)	Percentage deviation (%)
0.1	0.007178	0.742613	99.03	1	0.113036	0.742616	84.77
0.2	0.015133	0.742616	97.96	2	0.245542	0.742616	66.93
0.5	0.044293	0.742616	94.03	3	0.403521	0.742616	45.66
0,6	0.055962	0.742616	92.46	4	0.500747	0.742616	32.56
0.7	0.068668	0.742616	90.75	5	0.560577	0.742616	24.51
0.8	0.082426	0.742616	88.90	20	0.742797	0.742616	-0.024
0.9	0.097228	0.742616	86.90	33	0.742797	0.742616	-0.024

Fig. 5 illustrates the convergence of the solution obtained from the current analytical formulation for the reduction forces, in this case, the shear forces and the overturning moments. As in Fig. 6, it shows the variation of the amplitude of the shear coefficient C_f and that of the corresponding overturning moments. This figure also highlights the effect of fluid viscosity by varying the viscous damping coefficient ξ between 1% and 5% for a compressible-viscous fluid model. Similarly, Fig. 6 shows the variation of the amplitudes of the shear coefficient C_f and the corresponding overturning moment C_M as a function of the normalized excitation frequency.

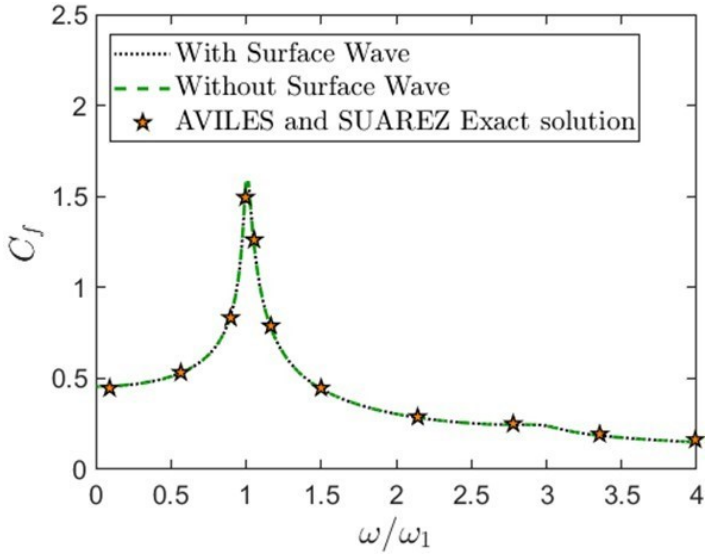

(a)

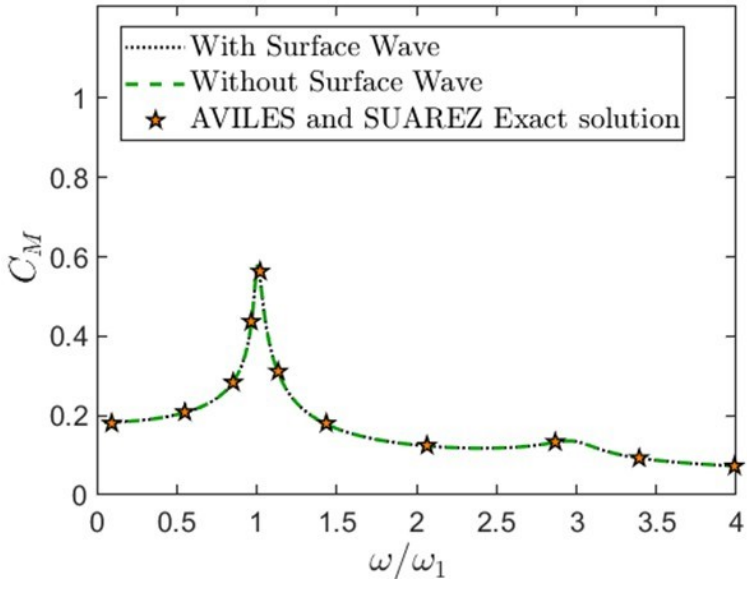

(b)

Table 4: Convergence of the present solution toward (Avilés and Suárez) exact solution for $c = 1$, $\theta = 15°$, and $\xi = 1\%$: (a) Variation of the force coefficient with frequency, (b) Variation of the moment coefficient with frequency

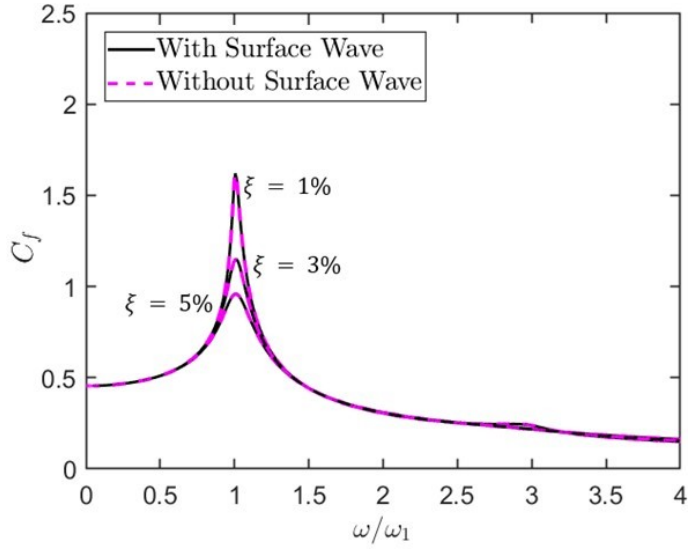

(a)

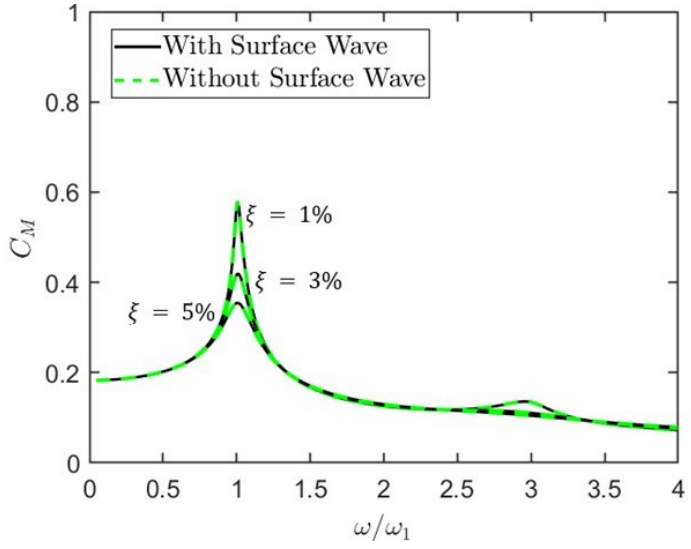

(b)

Table 5: Variation of the shear force coefficients and overturning moments as a function of normalized excitation frequency for $c = 1$, $\theta = 15°$, and different damping ratios; (a) Variation of the shear force coefficient; (b) Variation of the overturning moment coefficient

Interpretation

The results in Table 1 clearly show that as the excitation frequency decreases, the influence of surface gravity waves increases, resulting in significant reductions in the peak pressure coefficient. For the vertical dam, the reduction reaches 55.81% for a wave effect parameter of 0.4. For intermediate values, reductions of 24.51% (wave effect parameter of 0.2) and 40.85% (wave effect parameter of 0.3) are observed. These trends are consistent with the analytical results given by Wu and Yu (1989).

The combined effect of the excitation frequency and the inclination of the upstream face of the dam further reduces the hydrodynamic pressures. For a vertical dam, the pressure coefficient is 0.74. For an inclination of $\theta = 15°$, the pressure coefficient drops to 0.61. Taking into account the effect of surface gravity waves, it is further reduced to 0.52 when $CW = 0.2$ and to 0.38 for $CW = 0.4$.

For $\theta = 30°$, the combined effect is even more significant: from 0.74 (vertical dam), the pressure coefficient drops to 0.50 without surface waves, to 0.43 for $CW = 0.2$, and to 0.38 for $CW = 0.4$. These results clearly demonstrate that the greatest pressure reductions occur at lower excitation frequencies.

In table 2, for compressible and viscous fluids, the results indicate that at low frequencies, surface gravity waves significantly reduce the maximum pressures, whereas at higher frequencies the effect becomes negligible. This confirms that the compressibility of the fluid does not influence the energy dissipation mechanism generated by the presence of the surface wave effect.

The inclination of the upstream face constitutes a stabilizing mechanism for the dam, as it not only reduces hydrodynamic pressures but also allows the development of a stabilizing moment generated by the vertical component of the pressure force on the upstream face. For an inclination of $\theta = 15°$, for example (Table 1), at $CW = 0.4$, the maximum pressure reduction is 38.04% solely due to the effect of surface waves; this percentage increases to 49% if the effect of the inclination of the upstream face is simultaneously considered. These results are consistent with those of (Wu and Yu, 1989).

Avilés and Suárez (2010) also confirmed that inclination not only reduces pressures but also modifies the modal distribution of the reservoir.

Another aspect worth highlighting is that put forward by Da Silva and Pedroso (2019), according to which the total hydrodynamic response can be decomposed into two components:

(1) A so-called "conservative" component, associated with added mass and inertial effects,

(2) Another so-called "dissipative" component, linked to the damping effect generated by surface gravity waves.

In other words, in a slow regime, gravitational forces dominate, and the effect of surface gravity waves constitutes the main component of the hydrodynamic response. Neglecting these forces would lead to very large deviations (such as that corresponding to $\sigma = 0.1$, which approaches 100%). This confirms that in the slow regime, energy dissipation due to gravitational forces is significant.

In the fast regime, as F_r^2 increases, inertial forces dominate and the effect of surface gravity waves decreases rapidly. The pressure difference drops below 25% for $\sigma = 5$ for example, and becomes negligible at $\sigma = 20$. For this regime, the response is almost conservative, which is consistent with the observations of Wu and Yu (1989), and Avilés and Suárez (2010).

To conclude this analysis, it is interesting to address another mechanism of vibrational energy absorption: the effect of fluid viscosity. Fig. 6, shows that an increase in the damping ratio significantly reduces the hydrodynamic pressures around the resonance peaks. For this frequency range, the effect of surface waves is negligible, and viscosity dominates, controlling the resonance peaks by reducing the maximum hydrodynamic forces.

CONCLUSION

This study has highlighted the impact of surface gravity waves on the hydrodynamic response of a rigid dam subjected to horizontal harmonic excitation, taking into account the fluid's compressibility and viscosity. The analysis of the dam-reservoir system response was carried out using a semi-analytical approach based on a series of Trefftz functions.

The results obtained are very consistent with the trends in the specialized literature. They demonstrate that surface gravity waves have a significant impact on the hydrodynamic response of rigid dams, and that neglecting these effects, especially at low frequencies, would lead to an overall overestimation of hydrodynamic pressures that could exceed 30% (e.g., vertical dam). This is true, on the one hand.

On the other hand, the combination of the effect of surface waves with that of the inclination of the upstream face is revealing. At low frequencies, surface waves cause depressions near the free surface and redistribute the loads over the entire height of the dam. The combined effect results in a palpable reduction in hydrodynamic pressures, estimated to be approximately 39% for upstream slopes of 15° and at approximately 45% for upstream slopes of 30°. For higher frequencies, this effect gradually diminishes, giving way to that of viscous damping, which acts at resonance moments by limiting the amplitude of the maximum response.

Finally, the results suggest that the proposed semi-analytical framework provides a robust and efficient computational tool for evaluating hydrodynamic pressures under combined wave and damping effects.

Declaration of competing interest

The authors declare that they have no known competing interests or personal relationships that could have appeared to the work reported in this paper.

REFERENCES

AVILÉS J., LI X. (1998). Analytical–numerical solution for hydrodynamic pressures on dams with sloping face considering compressibility and viscosity of water, Computers and Structures, Vol. 66, Issue 4, pp. 481- 488.

AVILÉS J., SANCHEZ-SESMA F.J. (1986). Hydrodynamic pressures on dams with non-vertical upstream face, Journal of Engineering Mechanics, Vol. 112, pp. 1054-1061.

AVILÉS J., SUAREZ M. (2010). Effects of surface waves on hydrodynamic pressures on rigid dams with arbitrary upstream face, International Journal for Numerical Methods in Fluids, Vol. 62, pp. 1155-1168.

BELOUZ K., ZEREG S., MATALLAH, S. (2025). Modeling reservoir surface water temperature with neural networks and ANFIS, Larhyss Journal, No 64, pp. 57-81.

CHOPRA A.K. (1967). Hydrodynamic pressures on dams during earthquakes, Journal of the Engineering Mechanics Division, American Society of Civil Engineers (ASCE), Vol. 93, pp. 205-223.

CHWANG A.T. (1978). Hydrodynamic pressures on sloping dams during earthquakes, Journal of Fluid Mechanics, Part 2: "Exact theory", Vol. 87, pp. 343-348.

CHWANG A.T. (1981). Effect of stratification on hydrodynamic pressures on dams, Journal of Engineering Mathematics, Vol. 15, pp. 49-63.

DA SILVA S.F., PEDROSO L.J. (2019). Interaction dam-reservoir: Study of conservative and dissipative effects, Revista Ibracon de Estruturas e Materiais, Vol. 12, Issue 4, pp. 858-873.

DEUFLHARD P. (2011). Newton methods for nonlinear problems: Affine invariance and adaptive algorithms, Book, 2nd Edition, Springer, Series in Computational Mathematics 35, 424p.

FENVES G.L., CHOPRA A.K. (1984). Earthquake analysis of concrete gravity dams including reservoir bottom absorption and dam-water-foundation rock interaction, Earthquake Engineering & Structural Dynamics, Vol. 12, pp. 663-680.

GHOUINI F., KHA K.Q.N., BENAOUICHA M., SEGHIR A., GUILLOU S. (2024). FSI modeling of liquid sloshing in a flexible floating tank under regular wave effect, Larhyss Journal, No 59, pp. 53-68.

HALL J.F., CHOPRA A.K. (1972). Hydrodynamic pressures on dams during Earthquakes, Journal of the Engineering Mechanics Division, American Society of Civil Engineers (ASCE), Vol. 98, pp. 1535-1547

ICOLD (International Commission on Large Dams). (2016). Selecting seismic parameters for large dams, Bulletin No 148, Revisited Bulletin 72.

LIU P.L.F. (1986). Hydrodynamic pressures on rigid dams during earthquakes, Journal of Fluid Mechanics, Vol. 165, pp. 131-146.

MEHTA D., ACHOUR B., PASTAGIA J., AZAMATHULLA H., VERMA S. (2023). Review of reservoir operation, Larhyss Journal, No 56, pp. 193-214.

MEZENNER N., BENKACI T., BERMAD A., DECHEMI N. (2022). Dam reservoir operation optimization using genetic algorithm and principal component analysis simulation model - case of dam Ghrib, Larhyss Journal, No 51, pp. 145-160.

PANCHAL S.L., SURYANARAYANA T.M.V. (2025). Optimized operation of a multipurpose reservoir by evolutionary algorithm for Panam reservoir project in eastern Gujarat, India, Larhyss Journal, No 61, pp. 31-52.

REMINI B., TOUMI A. (2017). The Beni Haroun reservoir (Algeria) is it threatened by siltation? Larhyss Journal, No 29, pp. 249-263.

SHAIKH A.F., BHIRUD Y.L., MORE S.B., PAWAR A.D., VAIDYA O.V. (2024). Comparative analysis of optimization algorithms for reservoir operations: a case study on Ukai dam, Larhyss Journal, No 58, pp. 179-196.

TADJADIT A., TILIOUINE B. (2013). Analytical formulation of hydro-seismic forces at the fluid-structure interface of rigid dams with irregular upstream face under seismic excitations, Romanian Journal of Technical Sciences, Applied Mechanics, Vol. 58, Issue 3, pp. 287-298. (In French)

TADJADIT A., TILIOUINE B. (2018). Analytical expressions of hydro-seismic forces on dams, Periodica Polytechnica Civil Engineering, Vol. 62, Issue 2, pp. 480–493.

TADJADIT A. (2024). A semi-analytical method for parametric analysis of hydro-seismic forces on dams, Larhyss Journal, Vol. 58, pp. 21-30

TILIOUINE B., SEGHIR A. (1998). Fluid-structure models for dynamic studies of dam-water systems. 11th European Conference on Earthquake Engineering, September 6-11, Paris, France.

VERMA S., SAHU R.T., PRASAD A.D., VERMA M.K. (2023). Reservoir operation optimization using ant colony optimization a case study of Mahanadi reservoir project complex Chhattisgarh-India, Larhyss Journal, No 53, pp. 73-93.

WESTERGAARD H.M. (1933). Water pressures on dams during earthquakes (ASCE), Transactions of the American Society of Civil Engineers, Vol. 98, pp. 418-472.

WU Y.C., YU D.J. (1989). Trefftz method for hydrodynamic pressure on rigid dams with non-vertical upstream face, International Journal for Numerical Methods in Fluids, Vol. 9, pp. 1–7.

ZANGAR C.N. (1953). Hydrodynamic pressures on dams due to horizontal earthquakes, Proceedings of the Society of Experimental Stress Analysis, Vol. 10, pp. 93-102.

APPENDIX

Derivation of the dispersion relation

The problem formulated from the linearized wave equation for the potential function $\Phi(x, y, t)$ (or pressure p). We look for a steady-state solution using separation of variables:

$$\Phi(x,y,t)=X(x)\,Y(y)\,T(t) \tag{A1}$$

For a harmonic solution, the time part is $T(t) = e^{i\omega t}$.

We satisfy the bottom condition first because it is simple and restrictive. It immediately tells us the exact mathematical form of the vertical part of the solution. Applying this to our separated solution:

$$\frac{\partial \Phi}{\partial y}\Big|_{y=0} = X(x)\,\frac{dY}{dy}\Big|_{y=0}\,T(t)=0 \tag{A2}$$

Consider the possible solutions for $Y(y)$:

For $Y(y) = \sin(\lambda y)$, the derivative is $\lambda \cos(\lambda y)$, which equals ($\lambda \neq 0$) at ($y = 0$).

For $Y(y) = \cos(\lambda y)$, the derivative is $-\lambda \sin(\lambda y)$, which equals (0) at ($y = 0$). Hence, only $Y(y) = \cos(\lambda y)$ satisfies the boundary condition at the reservoir bottom. Applying the Poisson condition to:

$$\Phi(x,y,t) = \left[X(x)\cos(\lambda y)\right]e^{i\omega t} \tag{A3}$$

$$g\,\frac{\partial \Phi}{\partial y} = -g\,\lambda\left[X(x)\sin(\lambda y)\right]e^{i\omega t} \tag{A4}$$

Substitute into the boundary condition at the free surface:

$$\left[X\cos(\lambda y)\right]\left(-\omega^2 e^{i\omega t}\right) - g\,\lambda\left[X\sin(\lambda y)\right]e^{i\omega t} = 0 \tag{A5}$$

Factoring out the common terms:

$$-X e^{i\omega t}\left[\omega^2\cos(\lambda y) + g\,\lambda\sin(\lambda y)\right]=0 \tag{A6}$$

At $y = H_r$:

$$\omega^2\cos(\lambda H_r) + g\,\lambda\sin(\lambda H_r)=0 \tag{A7}$$

Rearranging and multiplying both sides of the equation by H_r:

$$\lambda_i H_r \tan\left(\lambda_i H_r\right) = -\frac{\omega^2 H_r}{g} \tag{A8}$$